Bidirectional reconfiguration and thermal tuning of microcantilever metamaterial device operating from 77 K to 400 K

Prakash Pitchappa, Manukumara Manjappa, Harish N. S. Krishnamoorthy, Yuhua Chang, Chengkuo Lee, and Ranjan Singh

Citation: Appl. Phys. Lett. **111**, 261101 (2017);
View online: https://doi.org/10.1063/1.5006836
View Table of Contents: http://aip.scitation.org/toc/apl/111/26
Published by the American Institute of Physics

Bidirectional reconfiguration and thermal tuning of microcantilever metamaterial device operating from 77 K to 400 K

Prakash Pitchappa,[1,2] Manukumara Manjappa,[1,2] Harish N. S. Krishnamoorthy,[1,2] Yuhua Chang,[3] Chengkuo Lee,[3] and Ranjan Singh[1,2,a)]
[1]*Division of Physics and Applied Physics, School of Physical and Mathematical Sciences, Nanyang Technological University, 21, Nanyang Link, Singapore 637371*
[2]*Center for Disruptive Photonic Technologies, The Photonics Institute, Nanyang Technological University, 50 Nanyang Avenue, Singapore 639798*
[3]*Department of Electrical and Computer Engineering, National University of Singapore, 4 Engineering Drive 3, Singapore 117576*

(Received 28 September 2017; accepted 7 December 2017; published online 26 December 2017)

We experimentally report the bidirectional reconfiguration of an out-of-plane deformable microcantilever based metamaterial for advanced and dynamic manipulation of terahertz waves. The microcantilever is made of a bimaterial stack with a large difference in the coefficient of thermal expansion of the constituent materials. This allows for the continuous deformation of microcantilevers in upward or downward direction in response to positive or negative temperature gradient, respectively. The fundamental resonance frequency of the fabricated microcantilever metamaterial is measured at 0.4 THz at room temperature of 293 K. With decreasing temperature, the resonance frequency continuously blue shifts by 30 GHz at 77 K. On the other hand, with increasing temperature, the resonance frequency gradually red shifts by 80 GHz and saturates at 0.32 THz for 400 K. Furthermore, as the temperature is increased above room temperature, which results in the downward actuation of the microcantilever, a significant resonance line-narrowing with an enhanced quality factor is observed due to tight field confinement in the metamaterial structure. The thermal control of the microcantilever possesses numerous inherent advantages such as enhanced tunable range (~37.5% in this work compared to previously reported microcantilever metamaterials), continuous tunability, and repeatable operations. The microcantilever metamaterial also shows high robustness to operate at cryogenic conditions and hence opens up the possibility of using meta-devices in harsh environments such as space, polar, and deep sea applications. *Published by AIP Publishing*. https://doi.org/10.1063/1.5006836

The advent of metamaterials has significantly aided in bridging the terahertz (THz) technological gap owing to the design versatility and large spectral scalability through engineering of the metamaterial unit cell geometry. This has led to the demonstration of various THz wave controls and manipulation, such as artificial magnetism,[1] unnaturally high refractive index,[2] perfect absorption,[3] chirality,[4] electromagnetically induced transparency,[5–9] high Q Fano resonances,[10] and many more.[11] With the advancement enabled by metamaterials in interacting with THz waves, the focus has currently shifted to actively controlled THz metadevices.[12] These THz metadevices are usually realized using active materials that are integrated into resonator geometry. The availability of large palette of naturally occurring active materials that respond to various external stimulus such as optical,[13,14] thermal,[15,16] electrical,[17,18] and magnetic fields[19] has enabled numerous THz metadevices with varying electro-optic performances.[20] Recently, the structural reconfiguration of the unit cell geometry using microelectromechanical systems (MEMS) technology provides a more straightforward means of achieving resonance tunability in metamaterials.[21–27] The microscale size of MEMS actuators matches with the unit cell dimension of THz metamaterials, thereby perfectly complementing each other. The reported THz MEMS metamaterials can be broadly categorized based on the plane of reconfiguration as: in-plane and out-of-plane reconfigurable metamaterials. In the case of in-plane reconfigurable metamaterials, the direction of actuation is along the plane containing the metamaterial resonators, and this allows for the dynamic reshaping of unit cell geometry and periodicity and hence the metamaterial response. Some of the widely used actuators for the in-plane reconfiguration in THz metamaterials include electrostatic comb drives,[22,23,28] electroactive polymers,[29] and mechanically stretchable substrates.[30] Alternatively, the out-of-plane reconfigurable metamaterial is formed by releasing a part of any resonator geometry from the substrate, which is then actively deformed with external control along the normal incident wave propagation direction. Various actuators are reported for realizing out-of-plane reconfigurable metamaterials such as electrostatically actuated microcantilevers and plates,[24–26,31–33] electrothermally actuated cantilevers,[34] thermally actuated bimorph stages,[21] pneumatically actuated stages,[35] and micro-spirals.[36] The huge array of MEMS actuators, combined with the possibility of using complementary metal-oxide-semiconductor (CMOS) compatible materials and processes, makes the MEMS metamaterial greatly attractive for realization of functional THz metadevices.[23] However, most of these MEMS metamaterials that are proposed for miniaturized solutions can only

a)Author to whom correspondence should be addressed: ranjans@ntu.edu.sg

provide unidirectional actuation relative to its initial rest position and also need metallic interconnects to provide the control signal, which greatly affects their electro-optic performance. Hence, the bidirectional reconfiguration of microcantilever metamaterials using thermal control will circumvent the above mentioned limitations and is a promising candidate for realizing high performance THz metamaterials.

In this paper, we experimentally demonstrate the bidirectional reconfiguration of MEMS metamaterials by integrating thermally reconfigurable bimaterial microcantilevers into resonator geometry. The bimaterial microcantilever is formed by selectively releasing the desired parts of the resonator geometry from the substrate while keeping the other part of the metamaterial fixed to the substrate. The bimaterial configuration of the microcantilever allows for the vertical deformation along upward and downward directions based on the gradient of temperature change. The resonance frequency of the metamaterial scales with the vertical displacement of the microcantilever. The opening up of an additional direction of out-of-plane reconfiguration (i.e., upward direction) along with the conventional downward reconfiguration, enhanced the tunable range by ~37.5%, compared to the conventional unidirectional and downward movable microcantilever metamaterials reported so far.[21,25–27,31,32,34,37] These metadevices were also characterized at cryogenic temperature of 77 K and showed strong resonance behavior. This crucial characteristic of the proposed microcantilever metamaterial is essential for the realization of high performance THz components such as modulators, filters, absorbers, and detectors to be used in rugged applications.

The proposed metamaterial is a 2D periodic array of electrical split ring resonators (ESRRs) with the geometrical dimensions shown in Fig. 1. The metamaterial is made of 300 nm thick aluminum (Al) on top of 50 nm thick aluminum oxide (Al_2O_3) dielectric, fabricated on a lightly p-doped silicon (Si) substrate with resistivity >1 Ω cm, using CMOS compatible process. Silicon-di-oxide (SiO_2) is used as the sacrificial layer, which is isotropically etched using vapor hydrofluoric acid to selectively release the central and tip parts of the ESRRs to form a pair of "T" shaped cantilevers in an ESRR unit cell as shown in Fig. 1(b). Upon release, the bimaterial cantilevers will curve upwards due to the residual stress between the Al and Al_2O_3 layers and can be qualitatively observed as increasing out-of-focus along the tip part in the optical microscopy image as shown in Fig. 1(b). The maximum vertical distance between the tip of the released microcantilever and Si substrate is termed as "release height (δ)" and was measured to be 2.7 μm at room temperature using a reflection based digital holographic microscope. The desired value of release height can be engineered by altering the length and thickness ratio of Al and Al_2O_3 layers of the cantilever.[37] The bimaterial layers with a large difference in their coefficient of thermal expansion allow for efficient control of release height through thermal stimulus. A change in out-of-plane displacement of the bimaterial cantilever ($\Delta\delta$) upon changing the temperature by ΔT with respect to room temperature (293 K) is given by the following equation:

$$\Delta\delta = \frac{3w_m w_d E_m E_d t_m t_d (t_m + t_d)(\alpha_m - \alpha_d)\Delta T.(cl)^2}{(E_m w_m t_m^2)^2 + (E_d w_d t_d^2)^2 + 2w_m w_d E_m E_d t_m t_d \left(2t_m^2 + 3t_m t_d + 2t_d^2\right)}, \quad (1)$$

where "w" is the width, "t" is the layer thickness, "E" is Young's modulus, "α" is the coefficient of thermal expansion (CTE), and the subscripts "m" and "d" represent the metal (Al) and dielectric (Al_2O_3) layers of the bimaterial cantilever, respectively. From Eq. (1), the two parameters which determine the direction of reconfiguration are the relative difference between the CTE values of constituent materials (i.e., $\Delta\alpha = \alpha_m - \alpha_d$) and the gradient of temperature change ($\Delta T = 293\,K - T$). The CTE value for thin film Al is $\alpha_m \sim 18.5 \times 10^{-6} K^{-1}$[38] and that of thin film Al_2O_3 is $\sim 4.22 \times 10^{-6} K^{-1}$.[39] Here, the Al layer is placed on top of Al_2O_3, and hence, $\Delta\alpha$ is always positive. Hence, the gradient of temperature change is exploited for achieving the bidirectional reconfiguration in microcantilevers. The room temperature of 293 K is considered as the reference point, as there is no external control signal provided. The optical image of the ESRR at 293 K is shown in Fig. 1(e). As the temperature is decreased from room temperature, the gradient of ΔT becomes positive, and the cantilever curves in the upward direction are shown in Fig. 1(d) for $\Delta T = +143$ K. With the increasing value of ΔT, the upward curvature increases and is seen as the larger out-of-focus of the cantilever for $\Delta T = +216$ K in Fig. 1(c). Alternatively, when the temperature is increased above room temperature, ΔT becomes negative and the cantilever deforms in the downward direction. When the temperature is increased to 350 K from 293 K, the cantilevers move closer to the Si substrate as shown in Fig. 1(f), and for 400 K, the cantilevers completely come in physical contact with the Si substrate and the entire ESRR along with released cantilevers, optically comes in-focus as shown in Fig. 1(g). This defines the limit for the maximum negative temperature gradient that can be utilized for the reported metadevice.

The THz response of the fabricated microcantilever metamaterial was characterized using the THz time domain spectroscopy (THz-TDS) system. A liquid nitrogen cryostat incorporated with a heating stage was integrated into the THz-TDS system to probe the positive and negative gradients of thermal stimulus. The cryostat with a temperature controller allowed for precise controlling of temperature from 77 K to 400 K. The THz wave excites the sample at normal incidence with the polarization direction along the in-plane gap of the

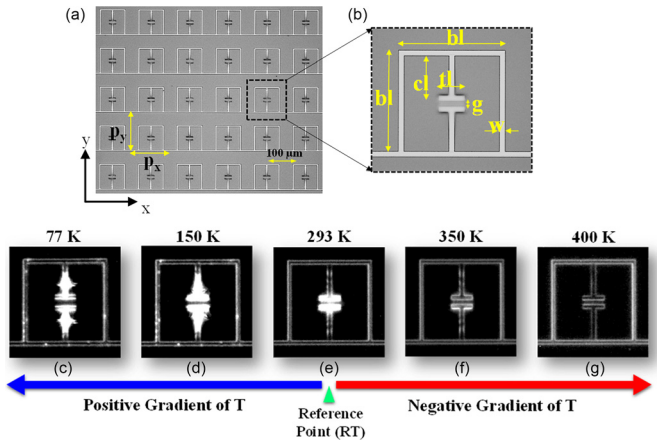

FIG. 1. Optical microscopy image of the fabricated ESRR microcantilever metamaterial—(a) ESRR array at room temperature with periodicities of $P_x = 120\,\mu m$ and $P_y = 120\,\mu m$ and (b) ESRR unit cell with geometrical parameter definitions: $bl = 80\,\mu m$, $cl = 34\,\mu m$, $tl = 20\,\mu m$, $g = 4\,\mu m$, and $w = 4\,\mu m$. The OM image of the ESRR unit cell at (c) 77 K, (d) 150 K, (e) 293 K (reference point), (f) 350 K, and (g) 400 K is shown.

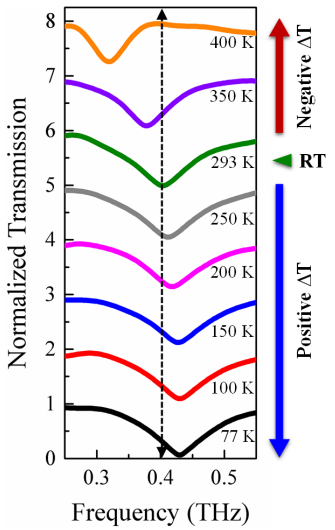

FIG. 2. Measured THz transmission response of the ESRR microcantilever metamaterial at varying temperatures. ΔT is defined as (293 K − T), and hence, temperature higher than 293 K represents negative ΔT and the resonance frequency is red shifted, whereas temperature lower than 293 K represents positive ΔT and the resonance frequency is blue shifted with respect to room temperature. The curves are plotted with vertical offset for better visibility.

ESRR (E_y). The transmission through the metamaterial was normalized with the transmission through the bare Si substrate of the same thickness to eliminate the influence of the Si substrate from metamaterial response. The normalized transmission response of the microcantilever metamaterial is shown in Fig. 2. At room temperature of 293 K, the fundamental resonance frequency (f_r) of ESRR was measured at 0.4 THz. With decreasing temperature, the resonance frequency continuously blue shifted to 0.42 THz at 77 K. On the other hand, with increasing temperature, the resonance frequency red shifted and saturated at 0.32 THz for 400 K. The change in resonance frequency of the fabricated metamaterial was calculated to be 0.02 THz for the complete range of positive gradient of temperature, $\Delta T = +216$ K. On the other hand, for the negative gradient range, the change in resonance frequency was 0.08 THz for the temperature change of $\Delta T = -107$ K. Hence, the shift in resonance frequency with the negative temperature gradient was significantly higher than that for the positive temperature gradient for the fabricated metamaterial. The measured electrical inductive-capacitive (ELC) resonance frequency (f_r) at varying temperatures is also shown in Fig. 3(a) that clearly highlights a larger shift in resonance frequency for the negative temperature gradient, relative to the case of the positive temperature gradient. The enhancement in the tunable range (ΔTR) due to the bidirectional (upward + downward) reconfiguration compared to the conventional microcantilever metamaterials which provides only the downward reconfiguration is calculated as $\Delta TR = (TR_{up+down} - TR_{down})/(TR_{down}) \times 100\%$. The enhancement in the tunable range (ΔTR) was calculated to be 37.5%, and this can be further altered by engineering the microcantilever dimensions and metamaterial design.[37] Additionally, temperature dependent resonance linewidth (Δf) and quality factor ($Q = f_r/\Delta f$) variations were also observed from the measured transmission spectra as shown in Fig. 3(b). With decreasing temperature, the linewidth and Q of the ELC resonance remained relatively unchanged. However, with increasing temperature, there was a strong narrowing of the resonance linewidth and an increase in the Q factor. In order to support these experimental observations, Finite Differential Time Domain (FDTD) based simulations were carried out.

The simulations were performed using Computer Software Technology (CST) under unit cell boundary conditions. For the material property, aluminum (Al) was modelled as a lossy metal with a DC conductivity of 3.56×10^7 S/m.[40] Aluminum oxide and silicon were modelled with dielectric constants of 9.5 and 11.7, respectively. The change in the release height ($\Delta\delta$) was analytically calculated using Eq. (1) and is shown as a green-circle plot in Fig. 4(a). Furthermore, finite element modelling (FEM) was carried out to confirm the analytical results, and the simulated results are shown as a pink-square plot in Fig. 4(a). The analytical method slightly overestimates the release height due to the approximation of the actual "T" shaped cantilever as a straight cantilever with a larger effective length of 42 μm. The bending profiles of the cantilever from FEM simulations are shown in insets for 77 K, 293 K, and 400 K, and they clearly show the upward deformation, reference deformation angle, and downward deformation of the microcantilever, relative to room temperature, respectively. In order to introduce the out-of-plane deformation in the FDTD simulations, a new parameter termed as the "release angle (θ)" was used, which defines the rotation angle between the microcantilever and the flat Si substrate based on the release height of the microcantilever at different temperatures. The inset of Fig. 4(b) shows the schematic definition of release height "δ" and release angle "θ." The release angle was calculated as $\theta = \sin^{-1}(\delta/cl)$ for varying temperatures and is shown in Fig. 4(b). With the calculated values of release angles at different temperatures, the resonance frequency of metamaterial was then simulated. The simulated resonance frequency of the ESRR microcantilever metamaterial at varying temperatures are shown along with the measured values in Fig. 3(a). The observed trend in the resonance frequency shift with

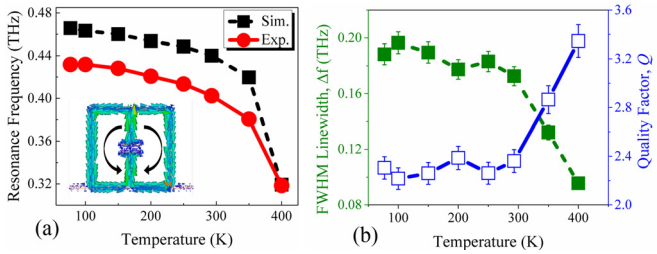

FIG. 3. (a) Simulated (black-dashed-square) and measured (red-solid-circle) resonance frequency, f_r, of the ESRR microcantilever metamaterial at varying temperatures from 77 K to 400 K. The inset shows the out-of-phase circulating current in the two SRRs forming the ESRR unit cell for E_y polarization of incident THz waves, signifying the excitation of the electrical inductive-capacitive (ELC) resonance mode of ESRR. (b) Linewidth, Δf (green-solid-square), and quality factor, $Q = f_r/\Delta f$ (blue-hollow-square), of the measured ELC resonance at different temperatures.

temperature is identical for simulated and measured results. The resonance frequency of the ESRR is given by $f_r = \omega_r/2\pi = (2\pi^2 \cdot L_{eff} \cdot C_{eff})^{-1/2}$, where L_{eff} and C_{eff} are the effective inductance and capacitance of the ESRR.[24,41] Also, $C_{eff} = C_i + C_o$, where C_i is the in-plane capacitance due to the split gap between the central part of ESRR, while C_o is the out-of-plane capacitance due to the air gap between the released cantilever and the Si substrate. Qualitatively, it can be understood that with increasing (decreasing) air gap, C_o will proportionately decrease (increase), which in turn causes the resonance frequency to blue shift (red shift). The mismatch between the simulated and measured values of f_r at all temperatures, except 400 K is primarily due to the assumption of the linear cantilever profile in simulation, but in reality, there is a non-linear curvature to the cantilever when it is released as shown in the left inset of Fig. 4(b). This approximation underestimates the C_o value compared to the actual case, and hence, the simulated f_r values are higher compared to the measured value. However, the measured and simulated resonance frequency of ESRR matches well for 400 K, when there is no out-of-plane air-gap ($\theta = 0$), since the simulation model represents the actual device more accurately as shown in the right inset of Fig. 4(b). It is important to note that even with mismatch in the exact values, this assumption of linear cantilever profile in simulation provides the necessary

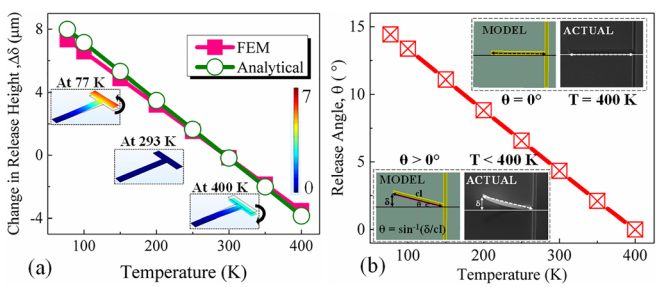

FIG. 4. (a) Depicts the analytically calculated values (green-circle) and FEM simulated (pink-square) values of change in the release height ($\Delta\delta$) with respect to temperatures. The insets show the FEM simulated change in the deformation profile of the microcantilever at 77 K, 293 K, and 400 K. (b) Depicts the analytically calculated values of the release angle with respect to temperature. The left inset shows the fabricated microcantilever suspended on top of the Si substrate at room temperature and the simulation model designed by assuming a linear profile of the cantilever with a specific release angle, θ. The right inset shows the fabricated microcantilever at 400 K and the accurate simulation model by using $\theta = 0°$.

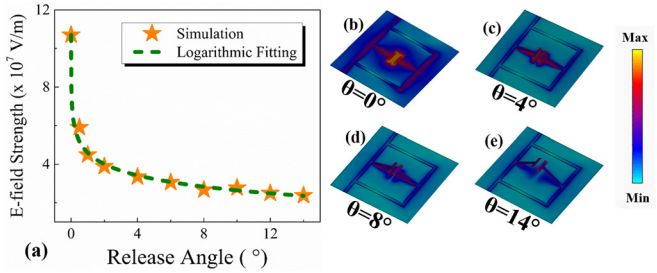

FIG. 5. (a) Simulated (orange-star) maximum electric field in the ESRR unit cell for varied release angles. The dotted green curve is fitted for the simulated values using the logarithmic function. The simulated electric field distribution for the ESRR unit cell for different release angles—(b) $\theta = 0°$, (c) $\theta = 4°$, (d) $\theta = 8°$, and (e) $\theta = 14°$.

insights for elucidating the physical mechanism of the light-matter interaction of the microcantilever metamaterial with incident THz waves at varying temperatures.

The electric field confinement in the ESRR microcantilever metamaterial was simulated for varying release angles. The electric field at each release angle was readout at the tip of the microcantilever, where the field confinement is the maximum and is shown in Fig. 5(a). The field confinement decreases logarithmically, signifying a more delayed decay due to the persistent coupling between the microcantilevers and Si substrate even at a larger release angle as shown in Fig. 5(a).[42] The absolute values of electric field confinement will vary in the actual device owing to the losses in the Si substrate, fabrication errors, inaccuracy in material properties, cantilever curvature profile, and other environmental factors that may arise in the experiments. The simulated electric field profile at varying release angles of 0°, 4°, 8°, and 14° is shown in Figs. 5(b)–5(e), respectively, and confirms the significant decrease in field confinement at larger release angles. The strong field confinement at a lower release angle is majorly due to the presence of high refractive index Si substrate. Due to this tight confinement of electric field at negative gradient of temperature, the radiative losses in the system are reduced significantly, thereby enabling higher quality factor resonance. However, when the cantilever moves away from the substrates, the field confinement is much lower and hence the resonance becomes highly radiative and hence reduces the quality factor as observed in the case of resonances for positive temperature gradient. Additionally, the conductivity of thin Al metal is also impacted by temperature but is not as significant as in the case of bulk Al and hence is neglected.[43]

In summary, a bidirectional reconfigurable microcantilever is experimentally reported as an active element, which is integrated into electrical split ring resonator geometry for advanced manipulation of terahertz waves. The access to the additional reconfiguration direction through thermal stimulus enabled enhancement in the tuning range by 37.5%, continuous tunability, and repeatable operation. The proposed approach is highly versatile in design, provides enhanced electro-optic performance, uses CMOS materials and processes, and is highly robust in operation, thus making it highly attractive for numerous high performance THz devices not only for commercial applications but also for niche and harsh environments such as space, deep-sea, and polar applications.

We would like to acknowledge Francesco Maddalena, Annalisa Bruno, and Cesare Soci for their support with optical imaging of microcantilever metamaterials at cryogenic temperatures. The authors acknowledge the research funding support from National Research Foundation (NRF) Singapore and Agence Nationale de la Recherche (ANR), France-NRF2016-NRF-ANR004 (M4197003).

[1]T.-J. Yen, W. Padilla, N. Fang, D. Vier, D. Smith, J. Pendry, D. Basov, and X. Zhang, Science **303**(5663), 1494–1496 (2004).
[2]M. Choi, S. H. Lee, Y. Kim, S. B. Kang, J. Shin, M. H. Kwak, K.-Y. Kang, Y.-H. Lee, N. Park, and B. Min, Nature **470**(7334), 369 (2011).
[3]H. Tao, N. I. Landy, C. M. Bingham, X. Zhang, R. D. Averitt, and W. J. Padilla, Opt. Express **16**(10), 7181–7188 (2008).
[4]E. Plum, J. Zhou, J. Dong, V. Fedotov, T. Koschny, C. Soukoulis, and N. Zheludev, Phys. Rev. B **79**(3), 035407 (2009).
[5]S.-Y. Chiam, R. Singh, C. Rockstuhl, F. Lederer, W. Zhang, and A. A. Bettiol, Phys. Rev. B **80**(15), 153103 (2009).
[6]R. Singh, C. Rockstuhl, F. Lederer, and W. Zhang, Phys. Rev. B **79**(8), 085111 (2009).
[7]M. Manjappa, S.-Y. Chiam, L. Cong, A. A. Bettiol, W. Zhang, and R. Singh, Appl. Phys. Lett. **106**(18), 181101 (2015).
[8]M. Manjappa, Y. K. Srivastava, A. Solanki, A. Kumar, T. C. Sum, and R. Singh, Adv. Mater. **29**(32), 1605881 (2017).
[9]M. Manjappa, Y. K. Srivastava, and R. Singh, Phys. Rev. B **94**(16), 161103 (2016).
[10]R. Singh, I. A. Al-Naib, M. Koch, and W. Zhang, Opt. Express **19**(7), 6312–6319 (2011).
[11]W. Withayachumnankul and D. Abbott, IEEE Photonics J. **1**(2), 99–118 (2009).
[12]K. Fan and W. J. Padilla, Mater. Today **18**(1), 39–50 (2015).
[13]W. J. Padilla, A. J. Taylor, C. Highstrete, M. Lee, and R. D. Averitt, Phys. Rev. Lett. **96**(10), 107401 (2006).
[14]H.-T. Chen, J. F. O'hara, A. K. Azad, A. J. Taylor, R. D. Averitt, D. B. Shrekenhamer, and W. J. Padilla, Nat. Photonics **2**(5), 295–298 (2008).
[15]J. Han and A. Lakhtakia, J. Mod. Opt. **56**(4), 554–557 (2009).
[16]Q.-Y. Wen, H.-W. Zhang, Q.-H. Yang, Y.-S. Xie, K. Chen, and Y.-L. Liu, Appl. Phys. Lett. **97**(2), 021111 (2010).
[17]H.-T. Chen, W. J. Padilla, J. M. O. Zide, A. C. Gossard, A. J. Taylor, and R. D. Averitt, Nature **444**(7119), 597–600 (2006).
[18]V. Savinov, V. A. Fedotov, S. Anlage, P. De Groot, and N. I. Zheludev, Phys. Rev. Lett. **109**(24), 243904 (2012).
[19]B. Jin, C. Zhang, S. Engelbrecht, A. Pimenov, J. Wu, Q. Xu, C. Cao, J. Chen, W. Xu, and L. Kang, Opt. Express **18**(16), 17504–17509 (2010).
[20]R. Singh, J. Xiong, A. K. Azad, H. Yang, S. A. Trugman, Q. Jia, A. J. Taylor, and H.-T. Chen, Nanophotonics **1**(1), 117–123 (2012).
[21]H. Tao, A. Strikwerda, K. Fan, W. Padilla, X. Zhang, and R. Averitt, Phys. Rev. Lett. **103**(14), 147401 (2009).
[22]W. M. Zhu, A. Q. Liu, X. M. Zhang, D. P. Tsai, T. Bourouina, J. H. Teng, X. H. Zhang, H. C. Guo, H. Tanoto, and T. Mei, Adv. Mater. **23**(15), 1792–1796 (2011).
[23]A. Liu, W. Zhu, D. Tsai, and N. I. Zheludev, J. Opt. **14**(11), 114009 (2012).
[24]F. Ma, Y.-S. Lin, X. Zhang, and C. Lee, Light: Sci. Appl. **3**(5), e171 (2014).
[25]P. Pitchappa, M. Manjappa, C. P. Ho, R. Singh, N. Singh, and C. Lee, Adv. Opt. Mater. **4**(4), 541–547 (2016).
[26]Z. Han, K. Kohno, H. Fujita, K. Hirakawa, and H. Toshiyoshi, Opt. Express **22**(18), 21326–21339 (2014).
[27]P. Pitchappa, C. P. Ho, L. Dhakar, and C. Lee, Optica **2**(6), 571–578 (2015).
[28]X. Zhao, K. Fan, J. Zhang, G. R. Keiser, G. Duan, R. D. Averitt, and X. Zhang, Microsyst. Nanoeng. **2**, 16025 (2016).
[29]T. Matsui, Y. Inose, D. A. Powell, and I. V. Shadrivov, Adv. Opt. Mater. **4**(1), 135–140 (2016).
[30]J. Li, C. M. Shah, W. Withayachumnankul, B. S.-Y. Ung, A. Mitchell, S. Sriram, M. Bhaskaran, S. Chang, and D. Abbott, Appl. Phys. Lett. **102**(12), 121101 (2013).
[31]M. Unlu, M. Hashemi, C. Berry, S. Li, S.-H. Yang, and M. Jarrahi, Sci. Rep. **4**, 5708 (2014).
[32]P. Pitchappa, C. P. Ho, Y. Qian, L. Dhakar, N. Singh, and C. Lee, Sci. Rep. **5**, 11678 (2015).
[33]X. Zhao, J. Schalch, J. Zhang, H. R. Seren, G. Duan, R. D. Averitt, and X. Zhang, in IEEE 30th International Conference on the Micro Electro Mechanical Systems (MEMS), 2017.
[34]C. P. Ho, P. Pitchappa, Y.-S. Lin, C.-Y. Huang, P. Kropelnicki, and C. Lee, Appl. Phys. Lett. **104**(16), 161104 (2014).
[35]A. Isozaki, T. Kan, H. Takahashi, K. Matsumoto, and I. Shimoyama, Opt. Express **23**(20), 26243–26251 (2015).
[36]T. Kan, A. Isozaki, N. Kanda, N. Nemoto, K. Konishi, H. Takahashi, M. Kuwata-Gonokami, K. Matsumoto, and I. Shimoyama, Nat. Commun. **6**, 8422 (2015).
[37]P. Pitchappa, C. P. Ho, L. Dhakar, Y. Qian, N. Singh, and C. Lee, J. Microelectromech. Syst. **24**(3), 525–527 (2015).
[38]W. Fang and C.-Y. Lo, Sens. Actuators, A **84**(3), 310–314 (2000).
[39]D. C. Miller, R. R. Foster, S.-H. Jen, J. A. Bertrand, S. J. Cunningham, A. S. Morris, Y.-C. Lee, S. M. George, and M. L. Dunn, Sens. Actuators, A **164**(1), 58–67 (2010).
[40]L. Cong, M. Manjappa, N. Xu, I. Al-Naib, W. Zhang, and R. Singh, Adv. Opt. Mater. **3**(11), 1537–1543 (2015).
[41]W. Padilla, M. Aronsson, C. Highstrete, M. Lee, A. Taylor, and R. Averitt, Phys. Rev. B **75**(4), 041102 (2007).
[42]M. Manjappa, S. P. Turaga, Y. K. Srivastava, A. A. Bettiol, and R. Singh, Opt. Lett. **42**(11), 2106–2109 (2017).
[43]R. Singh, D. Roy Chowdhury, J. Xiong, H. Yang, A. K. Azad, A. J. Taylor, Q. Jia, and H.-T. Chen, Appl. Phys. Lett. **103**(6), 061117 (2013).